Improved degradation of Orange II by Fe_3O_4/NiO/$NaHSO_3$ system under visible light irradiation

Yu Mei*

Key Laboratory of Pollution Exposure and Health Intervention of Zhejiang Province,
College of Biological and Environmental Engineering,
Zhejiang Shuren University,
Hangzhou, 310005, China
Email: imy1220@zjut.edu.cn
*Corresponding author

Bin Zhou

Zhejiang Environmental Monitoring Engineering Co. Ltd.,
Hangzhou, 310012, China
Email: weiweiwei321@163.com

Jianfeng Ma and Xinyu Zhang

School of Environmental and Safety Engineering,
Changzhou University,
Jiangsu, 213164, China
Email: jma@zju.edu.cn
Email: 24069571@qq.com

Abstract: Fe_3O_4/NiO composite oxides have been synthesised and characterised by various analytical techniques. Fe_3O_4/NiO was used as the catalyst to activate $NaHSO_3$, and supplemented with visible light illumination, which formed a novel photo-assisted Fenton-like system in degradation of dye in wastewater. By changing the calcination time of the precursor, three composite oxides are obtained. In degradation of the azo dye Orange II, several experimental results show that Fe_3O_4/NiO(8h) has the best adsorption and catalytic ability, 90% of the dye can be removed within 2 h in the Fe_3O_4/NiO(8h)/$NaHSO_3$ system. Also the mechanism of the degradation is discussed.

Keywords: Fe-Ni composite oxide; $NaHSO_3$; visible light; photocatalyst; degradation.

Reference to this paper should be made as follows: Mei, Y., Zhou, B., Ma, J. and Zhang, X. (2023) 'Improved degradation of Orange II by Fe_3O_4/NiO/$NaHSO_3$ system under visible light irradiation', *Int. J. Environment and Pollution*, Vol. 72, No. 1, pp.17–28.

Biographical notes: Yu Mei received her PhD in Environmental Engineering from Zhejiang Technology University of China in 2019. She is currently an Associated Professor in Zhejiang Shuren University. Her research interests include advanced oxidation and monitoring of new environmental pollutants.

Bin Zhou received his BSc from Zhejiang Technolgy University of China. His research interests include environmental monitoring.

Jianfeng Ma received his PhD in Environmental Engineering from Zhejiang University of China. He has been with the School of Environmental and Safety Engineering in Changzhou University as a Professor.

Xinyu Zhang received his BSc from Changzhou University. His research interests include developing of photocatalytic materials.

1 Introduction

Iron is able to activate hydrogen peroxide (H_2O_2), persulfate (PMS) or bisulfite (BS) in the homogeneous systems to produce corresponding active substances to degrade organic pollutants (Wang et al., 2019a; Sun et al., 2018; Zou et al., 2014; Bolobajev et al., 2015). One of the most classic reactions is Fenton reaction, in this system, Fe^{2+} reacts with H_2O_2 to generate strong oxidising hydroxyl radical (•OH) that can degrade organics rapidly, at the same time, Fe^{2+} is oxidised to Fe^{3+}, and Fe^{3+} can convert into Fe^{2+} through a series of reactions later (Zhu et al., 2020; Xu et al., 2019; Dou et al., 2018; Sirés et al., 2007). However, as the pH increases, Fe^{2+} not only cannot react with H_2O_2 to generate •OH, but also will produce ferric hydroxide precipitate, causing the loss of Fe^{2+} that leads to a continuous decrease in the reaction rate (Hou et al., 2018; Masomboon et al., 2010). Therefore, in order to maintain a steady rate of the reaction, bivalent iron salt will be added continuously. But the fluctuation of pH is inevitable, so Fe^{3+} in the system will precipitate continuously and the iron sludge will be on the increase. Similar to the traditional Fenton reaction, in the process of Fe^{2+} activating PMS or PDS, $SO_4^{\bullet-}$ replaces •OH to degrade organic pollutants (Yu et al., 2020; Xie et al., 2019; Ni et al., 2018). However, its defects are also similar to the Fenton reaction, it is difficult to regenerate Fe^{2+} after converting into Fe^{3+} (Li et al., 2016). Therefore, the homogeneous process of iron cannot be widely promoted. Chen et al. (2012) developed Fe(II)/sulphite for the degradation of organic dyes, after comparing with Fe(II)/PMS and Fe(II)/H_2O_2 , they found that Fe(II)/sulphite exceeded the others in the degradation of dyes, and $SO_4^{\bullet-}$ was confirmed as the main radical using tert-butanol through quenching experiment, •OH and $SO_5^{\bullet-}$ were also detected in the system. This phenomenon shows that the Fe(II)/sulphite system is one of the best methods for treating organic wastewater. However, the materials in the homogeneous system are difficult to recycle for reuse, and will cause secondary pollution, limiting the application of the homogeneous system in industry.

Studies have found that Fe_3O_4 has no obvious activation effect on H_2O_2 and $Na_2S_2O_8$, but it has a certain activation effect on $K_2S_2O_8$ (Lu et al., 2020; Pervez et al., 2020). Fe_3O_4 is used to activate $K_2S_2O_8$ to degrade sulfamethoxine, it is found that when the

dose of Fe_3O_4 is high enough, the degradation rate of pollutants is reduced. In addition, adding Fe_3O_4 in batches has a better effect than one-time addition. Fe_3O_4 not only has Fenton-like activity to activate persulfate, but also can act as a photocatalytic material (Laipan et al., 2016; Zhao et al., 2015; Kumar et al., 2013). Jia et al. (2015) prepared Fe_3O_4/g-C_3N_4 nanoparticles (NPs) using an uncomplicated electrostatic self-assembly method, and studied the oxidation process in Fenton reaction and Light-Fenton reaction. Contrast with the presence of Fe_3O_4 alone, Fe_3O_4/g-C_3N_4 nanoparticles are more efficient at degrading Rhodamine B (RhB), increasing by 20% and 90% respectively. The improvement of degradation efficiency is mainly due to the heterojunction formed between Fe_3O_4 and g-C_3N_4, which accelerates the charge transfer and inhibits the recombination of electrons and holes. Furthermore, Fe_3O_4/g-C_3N_4 material will not dissolve in most solvents, making it an excellent heterogeneous material. Xi et al. (2011) reported that magnetically Fe_3O_4/WO_3 core-shell visible-light photocatalyst showed higher performance compared with pure WO_3 or Fe_3O_4. It is noted that the active photocatalyst WO_3 with high surface area played an important role in capturing photons and converting them to photogenerated charges, and Fe_3O_4 acted as a charge collector which faciliated the charges transfer (Bazarjani et al., 2013). In addition, much attention has been focused on nickel oxide (NiO) nanoparticles including synthesis methods and photocatalytic performance of it. Hayat et al. (2011) studied that nickel oxide (NiO) nanoparticles with spherical shape and well-dispersed structure exhibited high photocatalytic performance as the phenol degradation rate could reach up to 97% within 60 min. Lakshmana et al. (2018) have synthesised CdS/NiO photocatalysts and its photocatalytic property was evaluated for H_2 generation under the condition of visible light irradiation. The NiO (thin shell) is an important active catalyst that induced efficient charge carriers transfer from CdS, which accelerated reduction reaction and enhancing hydrogen production (Zhang et al., 2021).

Herein, Fe_3O_4 is combined with NiO to prepare the Fe_3O_4/NiO composite material, which is applied to activate sodium bisulfite and enhance the photocatalytic activity. The Fe_3O_4/NiO/$NaHSO_3$ system is established to degrade Orange II dye wastewater. The ratio of iron and nickel was changed to optimise the degradation properties. Several characterisations have been carried out. The experimental conditions are changed to determine the influence of various factors, moreover, the active substances are determined by quenching experiments. After a comprehensive analysis of each result, the reaction mechanism of Fe_3O_4/NiO/$NaHSO_3$ system has been proposed.

2 Experimental

2.1 Chemicals

Nickel nitrate hexahydrate Ni $(NO_3)_2{\cdot}6H_2O$, iron (III) chloride hexahydrate ($FeCl_3{\cdot}6H_2O$), Orange II sodium salt, sodium bisulfite ($NaHSO_3$), ethanol, ethylene glycol, trisodium citrate (Na_3Cit), sodium acetate (NaOAc), ethanol, polyethanol, hydrochloric acid were purchased from the Sinopharm Chemical Reagent Co., Ltd. Shanghai, China. All the chemicals were analytical grade and were used as received.

2.2 Synthesis of Fe_3O_4/NiO

2.2.1 Prepration of Fe_3O_4

Firstly, 2.7 g iron (III) chloride hexahydrate ($FeCl_3 \cdot 6H_2O$) was fully dissolved in 80 ml ethylene glycol. After that 7.2 g sodium acetate (NaOAc), 1.44 g trisodium citrate (Na3Cit) and 2 g polyethanol mixed into the solution. The mixed solution was continuously stirred for 30 minutes. After that the mixed solution was put in a stainless steel reactor lined with polytetrafluoroethylene, and reacted at 200°C for 8 h in an oven. After the reaction was completed, the solid product collected was washed with ethanol and deionised water several times. The solid product was fully dried in an oven at 60°C to obtain Fe_3O_4.

2.2.2 Prepration of Fe_3O_4/NiO composite oxides

First, 100 mg Fe_3O_4 was put in 50 ml 0.2 M dilute hydrochloric acid, and then the mixed solution was sonicated for 10 min by an ultrasonic machine. After that, the Fe_3O_4 solid was separated and washed with absolute ethanol for use. 1.2 g nickel nitrate hexahydrate was fully dissolved in 72 ml ethylene glycol, Fe_3O_4 solid treated with dilute hydrochloric acid and a small amount of deionised water were also added to the solution. After sonication for 30 min, the mixed solution was put in a stainless steel reactor lined with polytetrafluoroethylene, and reacted at 160°C for 8 h in an oven. After that, the solid product was washed with ethanol and deionised water many times. The solid product was fully dried in an oven at 60°C to obtain precursor of Fe_3O_4/NiO composite oxide. Then, under the protection of N_2, the precursor was heated by the tubular furnace at 350°C for object time with a heating rate of 1°C min^{-1}. After calcination and grinding, Fe_3O_4/NiO composite oxide was obtained. The calcination time of the precursor could affect the thickness of the incrustation, therefore, the calcination time of the precursor was set to 2 h, 4 h and 8 h, respectively. Record the synthesised materials as Fe_3O_4/NiO (2h), Fe_3O_4/NiO (4h) and Fe_3O_4/NiO (8h).

2.2.3 Catalytic degradation of Orange II

Schematic illustration for the synthesis of Fe_3O_4/NiO/$NaHSO_3$ system is shown in Figure 1. The dye Orange II was selected as the target pollutant, the catalytic degradation ability of Fe_3O_4/NiO/$NaHSO_3$ system was studied in different experimental environments with or without visible light. The beaker containing 100 ml Orange II solution with a concentration of 50 mg L^{-1} was placed in a home-made photoreactor equipped with 5×24 W LED lamps, which can create darkness and visible light conditions, respectively. At room temperature, 50 mg Fe_3O_4/NiO powder and 100 mg $NaHSO_3$ were added to the dye solution to carry out the degradation reaction, and the magnetic stirrer kept stirring during the reaction. At fixed intervals, 5 ml solution was taken out and centrifuged, the centrifugal fluid was infiltration through a 0.22 μm filter and then loaded into a cuvette. The absorbance of the dye solution was measured at 484 nm with an ultraviolet-visible spectrophotometer UV-2450, Shimadzu.

Figure 1 Schematic illustration for the synthesis of Fe_3O_4/NiO/$NaHSO_3$ system (see online version for colours)

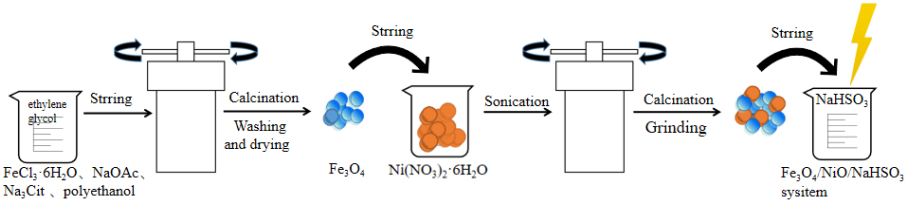

3 Results and discussion

3.1 Characterisation

Figure 2 is the X-ray diffraction pattern of Fe_3O_4 and Fe_3O_4/NiO samples. The characteristic diffraction peaks for the Fe_3O_4 and Fe_3O_4/NiO samples were detected at 2θ angles of 30.24°, 35.52°, 43.12°, 57.04° and 62.66°, which are respectively consistent with (440), (422), (400), (311) and (220) crystal planes of the Fe_3O_4 crystal with inverse spinel structure (JCPDS No. 19-629). This shows that the prepared two samples contain Fe_3O_4 crystal phase. In addition, no characteristic peak from any impurities was detected, indicating that the sample was pure Fe_3O_4 crystal phase. Compared with Fe_3O_4, Fe_3O_4/NiO also showed diffraction peaks at 2θ angles of 37.08° (111), 44.64° (200) and 51.62° (220), mainly corresponding to the diffraction peaks of NiO crystal (JCPDS No. 71-1179). Therefore, it could be speculated that the Fe_3O_4/NiO composite oxide was successfully synthesised.

Figure 2 XRD pattern of Fe_3O_4 and Fe_3O_4/NiO Fe_3O_4/NiO (4h) (see online version for colours)

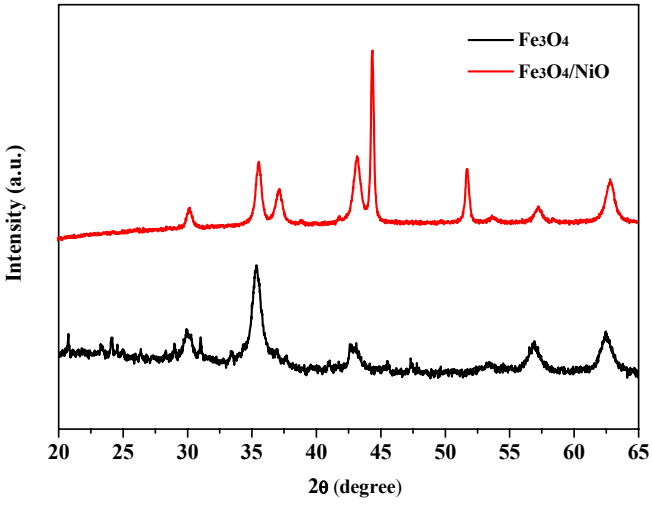

The SEM images of Fe_3O_4/NiO composite oxide at low magnification and high magnification are shown in Figure 3. It can be observed that most of the oxide exists like spherical nanoparticles of 250 nm. Since Fe_3O_4 was prepared separately, and nickel

nitrate and Fe_3O_4 were hydrothermally reacted to obtain Fe_3O_4/NiO, therefore NiO was either deposited on Fe_3O_4 or coexisted with Fe_3O_4. However, in the SEM images, the observed particle size is about 250 nm, and the diameter of the NiO particle is much smaller, it can be speculated that NiO coats the surface of Fe_3O_4 to form a shell structure. In addition, the SEM images of the Fe_3O_4/NiO composite oxide prepared in this experiment is similar to the Fe_3O_4@NiO shell core structure described in the previous reports (Kim et al., 2007). Because of its unique structural characteristics, the shell-core structure integrates the properties of both external and internal materials, so it is widely used in the field of catalysis. Therefore, Fe_3O_4/NiO composite oxide with excellent structure was successfully synthesised.

Figure 3 SEM images of Fe_3o_4/NiO

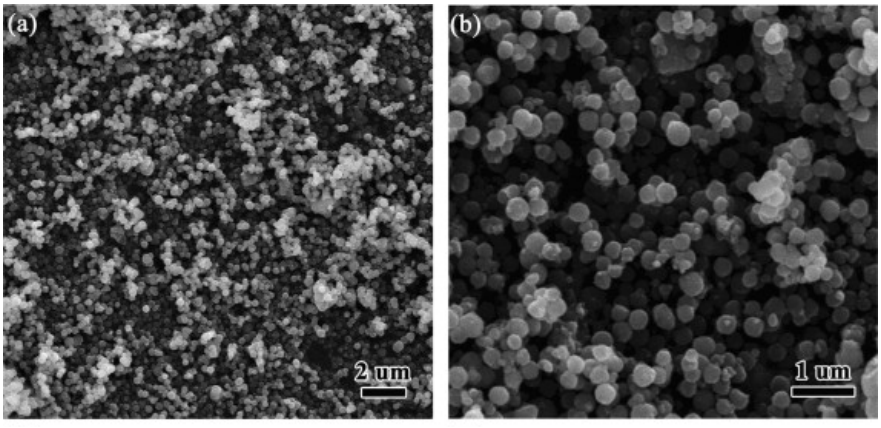

3.2 Degradation of Orange II with Fe_3O_4/NiO

3.2.1 Adsorption performance of Fe_3O_4/NiO for Orange II

Considering the special structure of Fe_3O_4/NiO, the adsorption properties of the materials were valuated. As shown in Figure 4, the composite materials such as Fe_3O_4/NiO (2h), Fe_3O_4/NiO (4h) and Fe_3O_4/NiO (8h) exhibited different properties on the adsorption of Orange II at the dark condition. Fe_3O_4/NiO (8h) had the best adsorption effect on Orange II. It was inferred that the precursor of Fe_3O_4/NiO obtained the optimal adsorption structure after calcining for 8 h. As the calcination time increases, the NiO shell of the Fe_3O_4/NiO composite oxide gradually thickens, and then the specific surface area of the NiO shell becomes larger and larger, which is more conducive to the dye adsorption. In addition, the excellent specific surface area can also increase the photocatalytic efficiency and shorten the catalytic degradation time.

3.2.2 Performance of Fe_3O_4/NiO/$NaHSO_3$ system for Orange II degradation

In the dark, 100 mg $NaHSO_3$ and 50 mg Fe_3O_4/NiO were added to Orange II solution to form the Fe_3O_4/NiO/$NaHSO_3$ system to degrade the dye. As shown in Figure 5, in the first 30 min, the degradation efficiency of different composite materials Fe_3O_4/NiO (2h), Fe_3O_4/NiO (4h) and Fe_3O_4/NiO (8h) to the dye was almost the same. As the reaction

progressed, it was found that the reaction system of Fe_3O_4/NiO (8h) as the catalyst had the degradation rate of 78.2%.

Figure 4 Adsorption kinetics of Orange II by different composite materials. conditions: Orange II 50 mg L^{-1}, Fe_3O_4/NiO 50 mg L^{-1} (see online version for colours)

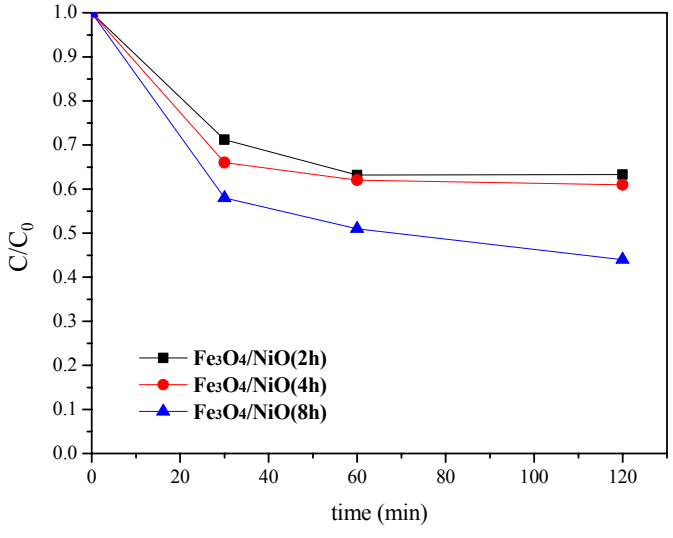

Figure 5 Degradation of Orange II with Fe_3O_4/NiO/$NaHSO_3$ system. conditions: Orange II 50 mg L^{-1}, Fe_3O_4/NiO 50 mg L^{-1}, $naHSO_3$ 100 mg L^{-1} (see online version for colours)

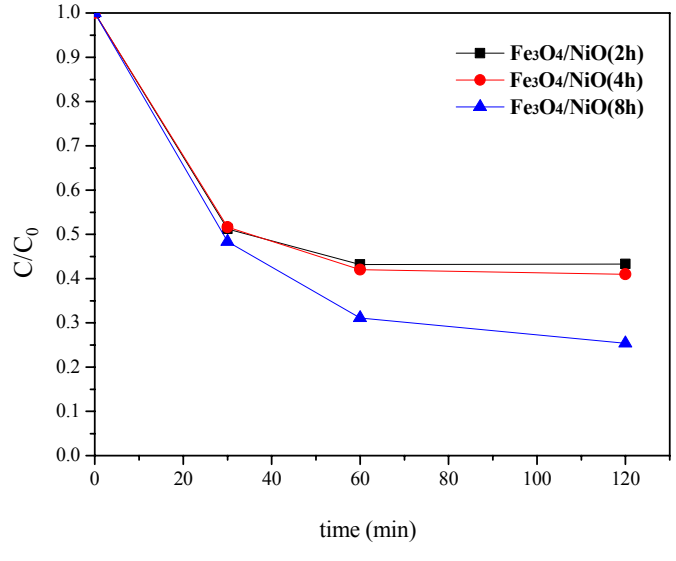

In order to verify the contribution of free radicals in the reaction, several free radical inhibitors were added to the Fe_3O_4/NiO/$NaHSO_3$ system, and the inhibitory effects of ethanol (EtOH) and tert-butanol (TBA) was found to be obvious (decrease to 35.5% and 67.8%), indicating that the main active substance in the system was $SO_4^{\bullet-}$. This also

explains why at the beginning of the synergistic effect of $NaHSO_3$ and Fe_3O_4/NiO, the degradation efficiency of the three materials with different calcination times are so close. That is, the iron in the material activates $NaHSO_3$ to generate $SO_4^{\bullet-}$ radicals, but the three materials differ only in the calcination time, and the mole ratio of iron to nickel are the same between the materials, so the amount of free radicals generated is also approximately the same, so the degradation effect is similar. However, as the reaction progresses, the adsorption of the core-shell structure of the material with optimised calcination time is gradually reflected, so the superiority of Fe_3O_4/NiO (8h) prepared by calcining for 8 h is more prominent.

3.2.3 Performance of Fe_3O_4/NiO/$NaHSO_3$ system for Orange II degradation under visible light

Figure 6 shows the degradation process of Orange II by Fe_3O_4/NiO/$NaHSO_3$ system under visible light. As shown in the figure, among the three composite oxide catalysts prepared by different calcination times, Fe_3O_4/NiO (8h) has the best catalytic performance. Due to the insufficient calcination time, the specific surface areas of the materials calcined by 2 h and 4 h calcination are small, the adsorption effect of these two materials are not as good as the material calcined by 8 h. Furthermore, since the small specific surface area can not provide enough photocatalytic degradation site, the catalytic effects of these two materials in the photo-assisted Fenton system are also inferior to Fe_3O_4/NiO (8h). The optimal system for this experiment is the Fe_3O_4/NiO (8h)/$NaHSO_3$ system under visible light, which can degrade 90% of Orange II during the reaction. The main degradation mechanism of this experiment is composed of two parts. On the one hand, iron activates bisulfite to form a Fenton-like system, which can generate sulphate radicals to effectively degrade organic pollutants. On the other hand, NiO with high specific surface area is excited by visible light for photocatalysis. In this study, the Shell structure Fe_3O_4/NiO composite oxides had been synthesised and used as the catalyst to activate $NaHSO_3$, and supplemented with visible light illumination, which formed a novel photo-assisted Fenton-like system in degradation of dye in wastewater. The results show that the Shell structure Fe_3O_4/NiO (8h) has the best adsorption and catalytic ability, 90% of the dye can be removed within 2 h in the Fe_3O_4/NiO (8h)/$NaHSO_3$ system. As can be seen in Table 1, the degradation efficiency of Orange II can reach 90.0% in Fe_3O_4/NiO/$NaHSO_3$ system within 120 min, which is higher than that of some previous studies (Table 1).

Table 1 Comparison of this work with previous report of similar composites

Sample	*Structural*	*Pollutant*	*Removal* (%)	*Reaction time* (min)
Fe_3O_4/NiO (This work)	Shell structure	Orange II	90.0	120
γ-Fe_2O_3/CeO_2 (Niu et al., 2021)	Rod-likemorphology	Tetracycline	84.0	120
Fe_3O_4 (Leng et al., 2014)	Spherical particles	Rhodamine B	80.0	120
Mn-doped SnO_2 (Babu et al., 2018)	Spherical particles	MO dye	90.0	250
Fe_2O_3-NiO-Cr_2O_3 (Ma et al., 2015)	Layered structure	Methylene blue	80.0	120

Figure 6 Degradation of Orange II with Fe_3O_4/NiO/$NaHSO_3$ system under visible light. conditions: Orange II 50 mg L^{-1}, Fe_3O_4/NiO 50 mg L^{-1}, $naHSO_3$ 100 mg L^{-1} (see online version for colours)

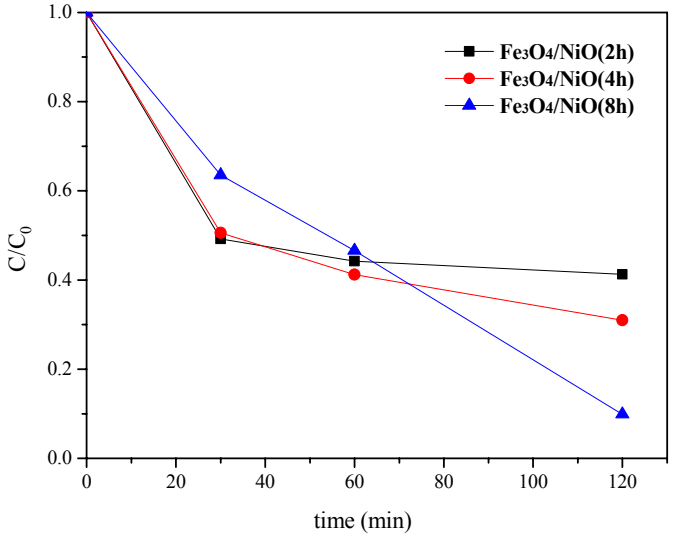

3.3 Mechanism

The catalytic mechanism of Orange II degradation by Fe_3O_4/NiO (8h)/$NaHSO_3$ system is proposed as follows:

The inhibitory effect of ethanol (EtOH) and tert-butanol (TBA) demonstrated the existence of $SO_4^{\bullet-}$ and •OH. Firstly, HSO_3^- was activated by Fe^{3+}, generating Fe^{2+} and $SO_3^{\bullet-}$ (Eq. (1)). Then, $SO_3^{\bullet-}$ could react with O_2 dissolved in water to produce $SO_5^{\bullet-}$, which can further react with HSO_3^- to form $SO_3^{\bullet-}$ and HSO_5^- (equations (2) and (3)) (Dou et al., 2020). Next, HSO_5^- could be activated by Fe^{2+}, accompanying with the generation of $SO_4^{\bullet-}$ (equation (4)). Furthermore, $SO_4^{\bullet-}$ could be changed to •OH by reaction with OH^- (equation (5)). The electron exchange between Ni^{2+} and Fe^{3+} in the Fe_3O_4/NiO could accelerate the conversation of Fe^{3+} to Fe^{2+}, which enhance the performance of the catalyst (equation (6)) (Zhang et al., 2017).

$$Fe^{3+} + HSO_3^- \rightarrow Fe^{2+} + SO_3^{\bullet-} + H^+ \quad (1)$$

$$SO_3^{\bullet-} + O_2 \rightarrow SO_5^{\bullet-} \quad (2)$$

$$SO_5^{\bullet-} + HSO_3^- \rightarrow SO_3^{\bullet-} + HSO_5^- \quad (3)$$

$$Fe^{2+} + HSO_5^- \rightarrow SO_4^{\bullet-} + Fe^{3+} \quad (4)$$

$$SO_4^{\bullet-} + OH^- \rightarrow \bullet OH + SO_4^{2-} \quad (5)$$

$$Ni^{2+} + Fe^{3+} \rightarrow Ni^{3+} + Fe^{2+} \quad (6)$$

The efficiency of Orange II degradation reached up to 90% under the visible light irridiation from 78.2% in the dark condition, which was attributed to the photocatalytic

ability of NiO. It was reported that nano NiO and Fe_3O_4 show high photocatalytic ability for degradation process (equations (6)–(11)) (Singh et al., 2017; Hayat et al., 2011; Wang et al., 2004). Moreover, NiO with high specific surface area is an important active catalyst that induced efficient charge carriers transfer from Fe_3O_4, which leads to rapid charge seperation and high degradation efficiency (Lakshmana et al., 2018).

$$NiO/Fe_3O_4 + hv \rightarrow e^- + h^+ \tag{7}$$

$$O_2 + e^- \rightarrow O_2^{\bullet -} \tag{8}$$

$$H_2O \rightarrow OH^- + H^+ \tag{9}$$

$$O_2^{\bullet -} + H^+ \rightarrow HOO\bullet \tag{10}$$

$$HOO\bullet + e^- \rightarrow HO_2^- \tag{11}$$

$$HOO^- + H^+ \rightarrow H_2O_2 \tag{12}$$

4 Conclusion

Several Fe_3O_4/NiO nanocomposites were prepared to study their ability to treat dye wastewater. Characterisation analysis shows that Fe_3O_4/NiO has a core-shell structure. Prolonging the calcination time of the precursor can optimise the core-shell structure of the material, thereby obtaining Fe_3O_4/NiO (8h) composite with high adsorption performance. Degradation experiments found that Fe_3O_4/NiO (8h) not only activates $NaHSO_3$ to produce $SO_4^{\bullet -}$ radicals to effectively degrade organic matter, but also has excellent photocatalytic performance. Under visible light, the degradation effect of Fe_3O_4/NiO (8h)/$NaHSO_3$ system on Orange II is greatly improved, and the removal rate reaches 90%. In addition, Fe_3O_4/NiO (8h) nanocomposite is magnetic, it can be highly dispersed in solution, and is also easy to recycle. In summary, Fe_3O_4/NiO (8h) nanocomposite is a catalyst with potential application value.

References

Babu, B., Kadam, A.N., Thirumala Rao, G., Lee, S.W., Byon, C. and Shim, J. (2018) 'Enhancement of visible-light-driven photoresponse of Mn-doped SnO_2 quantum dots obtained by rapid and energy efficient synthesis', *Journal of Luminescence*, Vol. 195, pp.283–289.

Bazarjani, M.S., Hojamberdiev, M., Morita, K., Zhu, G., Cherkashinin, G., Fasel, C., Herrmann, T. and Breitzke, H., Gurlo, A., Riedel, R. (2013) 'Visible light photocatalysis with c-$WO_{(3-x)}$/'$WO_3 \times H_2O$ nanoheterostructures in situ formed in mesoporous polycarbosilane-siloxane polymer', *Journal of the American Chemical Society*, Vol. 135, No. 11, pp.4467–4475.

Bolobajev, J., Trapido, M. and Dulova, N. (2015) 'Application of different techniques for activation of H_2O_2/Fe^{3+} system: a comparative study', *Journal of Advanced Oxidation Technologies*, Vol. 18, No. 2, pp.347–352.

Chen, L., Peng, X., Liu, J., Li, J. and Wu, F. (2012) 'Decolorization of Orange II in aqueous solution by an Fe (II)/sulfite system: replacement of persulfate', *Industrial and Engineering Chemistry Research*, Vol. 51, No. 42, pp.13632–13638.

Dou, R., Cheng, H., Ma, J. and Komarneni, S. (2020) 'Manganese doped magnetic cobalt ferrite nanoparticles for dye degradation via a novel heterogeneous chemical catalysis', *Materials Chemistry and Physics*, p.240.

Dou, R., Ma, J., Huang, D., Fan, C., Zhao, W., Peng, M. and Komarneni, S. (2018) 'Bisulfite assisted photocatalytic degradation of methylene blue by Ni-Fe-Mn oxide from MnO_4^- intercalated LDH', *Applied Clay Science*, Vol. 161, pp.235–241.

Hayat, K., Gondal, M.A., Khaled, M.M. and Ahmed, S. (2011) 'Effect of operational key parameters on photocatalytic degradation of phenol using nano nickel oxide synthesized by sol–gel method', *Journal of Molecular Catalysis A: Chemical*, Vol. 336, Nos. 1–2, pp.64–71.

Hou, Z., Ma, J., Fan, C., Peng, M. and Komarneni, S. (2018) 'Iron activated sodium bisulfite enhances generation of Mn (III) species through the MnO_2/bisulfite catalytic process', *Ceramics International*, Vol. 45, No. 1, pp.892–898.

Jia, X., Dai, R., Sun, Y., Song, H. and Wu, X. (2015) 'One-step hydrothermal synthesis of Fe_3O_4/g-C_3N_4 nanocomposites with improved photocatalytic activities', *Journal of Materials Science: Materials in Electronics*, Vol. 27, No. 4, pp.3791–3798.

Kim, S.H., Heo, C.J. and Lee, S.Y. (2007) 'Polymeric particles with structural complexity from stable immobilized emulsions', *Chemistry of Materials*, Vol. 19, pp.4751–4760.

Kumar, S., Surendar, T., Kumar, B., Baruah, A. and Shanker, V. (2013) 'Synthesis of magnetically separable and recyclable g-C_3N_4-Fe_3O_4 hybrid nanocomposites with enhanced photocatalytic performance under visible-light irradiation', *Journal of Physical Chemistry C*, Vol. 117, No. 49, pp.26135–26143.

Laipan, M.W., Zhu, R.L., Zhu, J.X. and He, H.P. (2016) 'Visible light assisted fenton-like degradation of Orange II on Ni_3Fe/Fe_3O_4 magnetic catalyst prepared from spent FeNi layered double hydroxide', *Journal of Molecular Catalysis A-Chemical*, Vol. 415, pp.9–16.

Lakshmana, R., Rao, N., Kumari, V.N., Ravi, M.M., Sathish, P. and Shankar, M.V. (2018) 'Effective shuttling of photoexcitons on CdS/NiO core/shell photocatalysts for enhanced photocatalytic hydrogen production', *Materials Research Bulletin*, Vol.101, pp.223–231.

Leng, Y., Guo, W., Shi, X., Li, Y., Wang, A., Hao, F. and Xing, L. (2014) 'Degradation of Rhodamine, B., by persulfate activated with Fe_3O_4: Effect of polyhydroquinone serving as an electron shuttle', *Chemical Engineering Journal*, Vol. 240, pp.338–343.

Li, T., Zhao, Z., Wang, Q., Xie, P. and Ma, J. (2016) 'Strongly enhanced fenton degradation of organic pollutants by cysteine: an aliphatic amino acid accelerator outweighs hydroquinone analogues', *Water Research*, Vol. 105, pp.479–486.

Lu, J., Zhou, Y., Lei, J., Ao, Z. and Zhou, Y. (2020) 'Fe_3O_4/graphene aerogels: a stable and efficient persulfate activator for the rapid degradation of malachite green', *Chemosphere*, Vol. 251, pp.1–11.

Ma, J.F., Ding, J.F., Yu, L.M., Li, L.Y., Kong, Y. and Komarneni, S. (2015) 'Synthesis of Fe_2O_3–NiO–Cr_2O_3 composites from niFe-layered double hydroxide for degrading methylene blue under visible light', *Applied Clay Science*, Vol. 107, pp.85–89.

Masomboon, N., Ratanatamskul, C. and Lu, M-C. (2010) 'Mineralization of 2,6-dimethylaniline by photoelectro-Fenton process', *Applied Catalysis A General*, Vol. 384, No. 2, pp.128–135.

Ni, Q., Ma, J., Fan, C., Kong, Y., Peng, M. and Komarneni, S. (2018) 'Spinel-type cobalt-manganese oxide catalyst for degradation of Orange II using a novel heterogeneous photo-chemical catalysis system', *Ceramics International*, Vol. 44, pp.19474–19480.

Niu, L., Zhang, G., Xian, G., Ren, Z., Wei, T., Li, Q., Zhang, Y. and Zou, Z. (2021) 'Tetracycline degradation by persulfate activated with magnetic γ-Fe_2O_3/CeO_2 catalyst: performance, activation mechanism and degradation pathway', *Separation Purification Technology*, Vol. 259, p.118156.

Pervez, N., He, W., Zarra, T., Naddeo, V. and Zhao, Y. (2020) 'New sustainable approach for the production of Fe_3O_4/graphene oxide-activated persulfate system for dye removal in real wastewater', *MDPI in Water*, Vol. 12, pp.1–9.

Singh, K.K., Senapati, K.K., Borgohain, C. and Sarma, K.C. (2017) 'Newly developed Fe_3O_4–Cr_2O_3 magnetic nanocomposite for photocatalytic decomposition of 4-chlorophenol in water', *Journal of Environmental Sciences*, Vol. 52, pp.333–40.

Sirés, I., Garrido, J.A., María, R., Brillas, R.E., Oturan, N., and Oturan, M.A. (2007) 'Catalytic behavior of the Fe^{3+}/Fe^{2+} system in the electro-fenton degradation of the antimicrobial chlorophene', *Applied Catalysis B: Environmental*, Vol. 72, No. 3, pp.382–394.

Sun, M., Chu, C., Geng, F., Lu, X., Qu, J., Crittenden, J., Elimelech, M. and Kim, J. (2018) 'Reinventing fenton chemistry: iron oxychloride nanosheet for pH-insensitive H_2O_2 activation', *Environmental Science and Technology Letters*, Vol. 5, pp.1–8.

Wang, H., Guo, W., Yin, R., Du, J., Wu, Q., Luo, H., Liu, B., Sseguya, F. and Ren, N. (2019a) 'Biochar-induced fe (III) reduction for persulfate activation in sulfamethoxazole degradation: insight into the electron transfer, radical oxidation and degradation pathways', *Chemical Engineering Journal*, Vol. 362, pp.561–569.

Wang, X., Song, J., Gao, L., Jin, J., Zheng, H. and Zhang, Z. (2004) 'Optical and electrochemical properties of nanosized NiO via thermal decomposition of nickel oxalate nanofibres', *Nanotechnology*, Vol. 16, No. 1, p.37.

Xi, G., Yue, B., Cao, J. and Ye, J. (2011) 'Fe_3O_4/WO_3 hierarchical core-shell structure: high-performance and recyclable visible-light photocatalysis', *Chemistry*, Vol. 17, No. 18, pp.5145–5154.

Xie, P., Zhang, L., Chen, J., Ding, J., Wan, Y., Wang, S., Wang, Z., Zhou, A. and Ma, J. (2019) 'Enhanced degradation of organic contaminants by zero-valent iron/sulfite process under simulated sunlight irradiation', *Water Research*, Vol. 149, pp.169–178.

Xu, L., Meng, L., Zhang, X., Mei, X., Guo, X., Li, W., Wang, P. and Gan, L. (2019) 'Promoting Fe^{3+}/Fe^{2+} cycling under visible light by synergistic interactions between P25 and small amount of fenton reagents', *Journal of Hazardous Materials*, Vol. 379, pp.43–52.

Yu, X., Sun, J., Li, G., Huang, Y., Li, Y., Xia, D. and Jiang, F. (2020) 'Integration of $\bullet SO_4^-$-based AOP mediated by reusable iron particles and a sulfidogenic process to degrade and detoxify Orange II', *Water Research*, Vol. 174, pp.1–9.

Zhang, H., Liu, J., Ou, C., Shen, F.J., Yu, H., Jiao, Z., Han, W., Sun, X., Li, J. and Wang, L. (2017) 'Reuse of fenton sludge as an iron source for niFe_2O_4 synthesis and its application in the fenton-based process', *Journal of Environmental Sciences (China)*, Vol. 53, pp.1–8.

Zhang, X.R., Mei, Y., Cheng, H., Ma, J.F., Zhu, F. and Komarneni, S. (2021) 'Activation of $K_2S_2O_8$ by ni–ce composite oxides for the degradation of Orange II with visible light assistance', *Materials Chemistry and Physics*, Vol. 270, p.124784.

Zhao, H., Qian, L., Lv, H., Wang, Y. and Zhao, G. (2015) 'Introduction of a Fe_3O_4 core enhances the photocatalytic activity of MIL-100 (Fe) with tunable shell thickness in the presence of H_2O_2', *ChemCatChem*, Vol. 7, No. 24, pp.4148–4155.

Zhu, B.Y., Cheng, H., Ma, J.F., Qin, Y., Kong, Y. and Komarneni, S. (2020) 'Bi2MoO6 microspheres for the degradation of Orange II by heterogeneous activation of persulfate under visible light', *Materials Letters*, Vol. 261, p.127099.

Zou, X., Zhou, T., Mao, J. and Wu, X. (2014) 'Synergistic degradation of antibiotic sulfadiazine in a heterogeneous ultrasound-enhanced Fe^0/persulfate fenton-like system', *Chemical Engineering Journal*, Vol. 257, pp.36–44.